Clays and Clay Minerals, Vol. 54, No. 3, 275–294, 2006.

MINERALOGY AND GEOCHEMISTRY OF THE HOST-ROCK ALTERATIONS ASSOCIATED WITH THE SHEA CREEK UNCONFORMITY-TYPE URANIUM DEPOSITS (ATHABASCA BASIN, SASKATCHEWAN, CANADA). PART 1. SPATIAL VARIATION OF ILLITE PROPERTIES

EMMANUEL LAVERRET[1], PATRICIA PATRIER MAS[1,*], DANIEL BEAUFORT[1], PHILIPPE KISTER[2], DAVID QUIRT[3], PATRICE BRUNETON[4] AND NORBERT CLAUER[5]

[1] HydrASA, UMR CNRS 6532, University of Poitiers, 40 Avenue du Recteur Pineau, 86022 Poitiers Cedex, France
[2] UMR CNRS 7566 G2R-CREGU, UHP, BP 239, 54506 Vandœuvre-lès-Nancy Cedex, France
[3] Saskatchewan Research Council, 15 Innovation Boulevard, Saskatoon, Saskatchewan, S7N 2X8, Canada
[4] COGEMA, Business Unit Mines, 2, rue Paul Dautier, BP 4, 78141 Velizy Cedex, France
[5] Centre de Géochimie de la Surface, 1 Rue Blessig, 67084 Strasbourg Cedex, France

Abstract—Unconformity-related uranium deposits, which represent a significant high-grade uranium resource, are systematically surrounded by a host-rock alteration halo enriched in clay minerals. Illite is often the major clay mineral component of the halo and it displays a variable crystal structure. New data are provided on the crystal structure and the chemistry of illite encountered within and outside of the alteration halo surrounding the Shea Creek deposit. Two illite populations were distinguished using textural and structural criteria: samples rich in the *tv*-1*M* polytype display thin (sub-micrometer) and 'hairy' shapes, while samples richer in the *cv*-1*M* polytype contain illites with rigid lath-like shapes several micrometers wide. In barren 'regional' sandstone, the trends with depth of the textural and microstructural properties of illite particles are: (1) an increase of particle size, (2) an evolution to a more isometric form, and (3) a dominance of the *cv*-1*M* polytype over the *tv*-1*M* polytype. These trends record diagenetic processes under conditions of deep burial and differ from those observed in altered sandstone around the uranium mineralization. The altered sandstone is characterized by enrichment in the *tv*-1*M* polytype near the unconformity and/or brittle structural features. This *tv*-1*M* illitization took place in response to structurally-controlled infiltration of basement rocks by diagenetic brines which were further recycled after interaction into the overlying basin. Variations of the illite structural and textural properties may result from nucleation/growth kinetics and may be indicative of a change in the flow regime, and/or a change of saturation state of the fluid *vs.* illite. The *tv*-1*M* illite may be favored in environments characterized by a high fluid/rock ratio and a high supersaturation state of the fluids in proximity to mineralization.

Key Words—Athabasca Basin, Crystal Chemistry, Crystal Form, Crystal Structure, Host-rock Alteration, Illite, Kaolin Minerals, Sudoite, Unconformity-type Uranium Deposit.

INTRODUCTION

Unconformity-type or unconformity-related uranium deposits (URUD) represent the most significant high-grade, low-cost uranium resource in the world and still constitute major exploration targets. Located near the unconformity between Middle Proterozoic sandstones and lower Proterozoic metasediments, the URUDs are surrounded by a host-rock alteration halo in which clay minerals dominate alteration features and clay minerals have been studied extensively around the deposits located in the Athabasca and Thelon basins of Canada (Hoeve and Quirt, 1984; Kotzer and Kyser, 1995; Renac *et al.*, 2002; Quirt, 2003, among others) and in the McArthur basin of Australia (Gustafson and Curtis, 1983; Patrier *et al.*, 2003; Beaufort *et al.*, 2005).

* E-mail address of corresponding author:
patricia.patrier@hydrasa.univ-poitiers.fr
DOI: 10.1346/CCMN.2006.0540301

Illite is considered to be a diagnostic pathfinder mineral for URUDs because it is typically the major clay mineral component in the alteration halo. Variations in illite crystal structure and/or chemistry have been used to determine the nature of the alteration processes and the paleoconditions of the water-rock interaction processes related to the U deposition (Hoeve and Sibbald, 1978; Hoeve and Quirt, 1984; Kotzer and Kyser, 1995).

Previous investigations suggest that the crystal structure of illite from the Athabasca Basin is variable and not well characterized. Hoeve and Quirt (1984), Ey *et al.* (1985), Halter (1988), and Quirt (2003) note that illite with $2M_1$ and 1*M* polytypes predominates, with the 3*T* polytype being associated with U mineralization. However, Drits *et al.* (1993) demonstrated that illite in the alteration halo surrounding the Cigar Lake deposit is dominantly of the 1*M* polytype with locations of the vacant octahedral sites varying as a function of the distance from the ore body. They determined that the Cigar Lake illite, previously identified as 3*T* illite, is actually 1*M* illite with octahedral *cis*-vacant sites (*cv*-1*M*

Copyright © 2006, The Clay Minerals Society

polytype) and they questioned the existence of the 3*T* polytype in such geological environments.

The aim of this paper is to provide new mineralogical and chemical data for illite encountered within and outside of the alteration halo surrounding the Shea Creek U deposits (western Athabasca Basin), where massive U mineralization has been discovered at the unconformity between the Athabasca Group sandstone and sub-Athabasca crystalline basement rocks. The spatial variations in both the host-rock alteration petrography and the illite characteristics (crystal structure, mineral chemistry, and texture) are used to determine and interpret the 'diagenetic-to-hydrothermal' transition observed in the vicinity of the Shea Creek deposits, as for other deposits in the Athabasca Basin (Hoeve and Sibbald, 1978; Hoeve and Quirt, 1984; Kotzer and Kyser, 1995; Quirt, 2003; among others). The overall spatial distribution and normative mineralogical composition of the host-rock alteration minerals for the Shea Creek deposits are addressed in a related paper (Kister *et al*., 2006, this issue).

REGIONAL GEOLOGY

The Athabasca Basin is an intracratonic (*sensu lato*) basin located in northern Saskatchewan and Alberta (Figure 1). It covers an area of ~100,000 km^2 and is undeformed except by faulting and by the Carswell meteorite impact structure (Hoeve and Quirt, 1984, 1987; Ramaekers, 1990; Ramaekers *et al.*, 2001). It unconformably overlies a crystalline basement complex comprising highly-deformed, medium- to high-grade metamorphic Archean granitoid gneisses, Paleoproter-ozoic metasediments and Hudsonian intrusives belonging to the west-central part of the Canadian Shield. The Rae and Hearne provinces represent the major litho-structural subdivisions of the basement in this part of the Canadian Shield. This basin contains the preserved portion of the unmetamorphosed Athabasca Group, presently consisting of up to 2300 m of three fining-upward orthoquartzitic clastic sequences bounded by unconformities: the lower Fair Point sequence, the Manitou Falls-Wolverine Point sequence, and the upper Locker Lake-Douglas sequence (Hoeve and Quirt, 1984; Ramaekers, 1990; Ramaekers *et al.*, 2001). These orthoquartzitic sequences are dominantly composed of variably hematitic, medium- to coarse-grained, fluviatile, quartz-rich sandstones, conglomerates and minor siltstones. Two silty marine to lacustrine clastic formations (Wolverine Point and Douglas Formations, respectively) cap the last two sequences and the preserved stratigraphic sequence is capped by dolomite (Carswell Formation). The depositional ages of the Athabasca Group sediments are Mesoproterozoic, 1720−1650 Ma (Cumming *et al.*, 1987; Rainbird *et al.*, 2002).

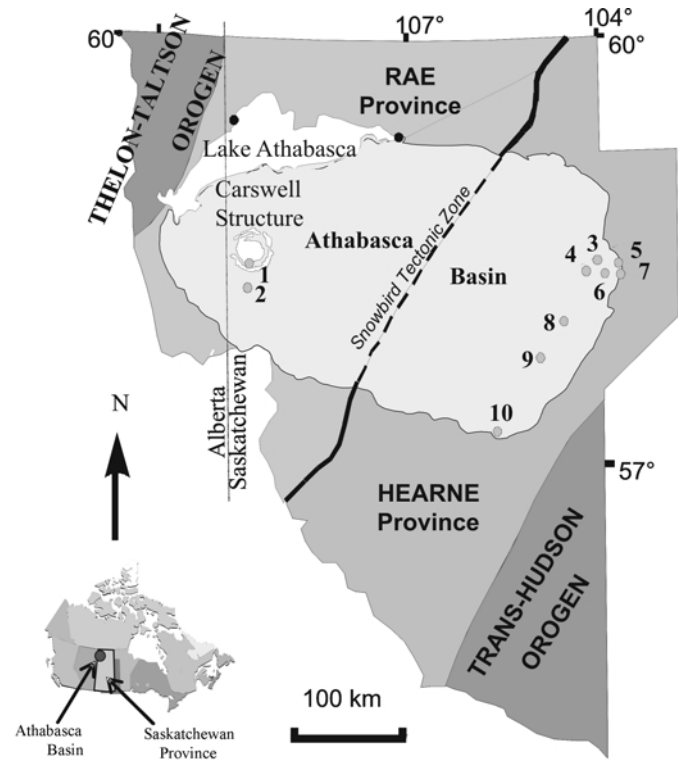

Figure 1. Location map of the Athabasca Basin (northern Saskatchewan, Canada). The major U deposits are: Cluff Lake (1), Shea Creek (2), Dawn Lake (3), Midwest (4), Collins Bay (5), McClean Lake and Sue (6), Rabbit Lake (7), Cigar Lake (8), McArthur River (9), and Key Lake (10).

The Shea Creek region (Figure 1) is located in the western part of the Athabasca Basin, 15 km south of the Carswell meteorite impact structure, and 300 km west of the major U deposits of the Eastern Athabasca region. The sedimentary cover in the study area varies in thickness from ~400 m in the southernmost part to ~760 m in the north. Six formations of the Athabasca Group are distinguished within the Shea Creek region from bottom to top: the Manitou Falls c and d (MFc, MFd), Lazenby Lake (LzL), Wolverine Point a and b (WPa, WPb), Locker Lake (LL), and the Otherside (OS) Formations (Table 1). This sedimentary succession is covered by recent glacial sediments.

The detrital mineralogy of the Athabasca Group sediments in the Shea Creek region is similar to that described for the eastern part of the basin (Hoeve and Quirt, 1984; Hoeve *et al*., 1985; Ramaekers, 1990; Quirt, 2003), being dominated by monocrystalline quartz grains with minor amounts of polycrystalline quartz and rare biotite inclusions. Zircon, Fe-tourmaline, Fe-Ti oxides, and rare detrital white micas occur as ubiquitous trace accessory minerals. No feldspar mineral grains were observed and the existence of such detrital minerals in the Athabasca basinal fill is questionable (Hoeve and Quirt, 1984; Ramaekers, 1990; Laverret, 2002; Quirt, 2003).

The Athabasca Group underwent deep burial with a maximum depth of between 4 and 5 km (Pagel, 1975; Hoeve and Quirt, 1984; Kotzer and Kyser, 1995). The major ubiquitous diagenetic processes have been pore sealing by quartz overgrowths and recrystallization and neoformation of clay minerals. The dominant clay mineral is kaolin (kaolinite-to-dickite conversion series), which was replaced to varying extents by authigenic illite during deep burial (Hoeve and Quirt, 1984; Laverret, 2002; Quirt, 2003). The diagenetic mineral assemblage also includes Fe minerals (dominantly hematite; locally siderite and/or pyrite), dravite overgrowths on detrital tourmaline, and crandallite-group aluminum phosphate sulfate (APS) minerals.

In the Shea Creek region, the sub-Athabasca basement consists of a graphitic metasedimentary unit, including pelitic gneisses and garnetite, intercalated between two felsic orthogneiss units (Pagel and Svab, 1985; Card, 2002; Brouand *et al*., 2003). The metasedimentary unit was thrust over the lower felsic gneiss unit (Rippert *et al.*, 2000; Lorilleux *et al.*, 2002). The basement rocks have undergone retrograde metamorphism (*i.e.* biotite and garnet chloritization, feldspar sericitization) attributed to isostatic uplift of the rocks during the Trans-Hudson orogen (1880−1760 Ma; Pagel and Svab, 1985; Halter, 1988; Chiarenzelli *et al.*, 1998). A regolith (paleoweathering) profile caps the basement lithologies and ranges from 10 to 20 m in thickness. At present, a zoned, clay-rich kaolinitic ± hematitic profile is partly preserved marking the regolith horizon (Hoeve and Quirt, 1984; Halter, 1988; Quirt, 2003). This clay-rich layer was later modified by diagenetic fluids circulating within the overlying sandstones (Kotzer and Kyser, 1995).

The Shea Creek uranium deposits, consisting of the Anne and Colette ore zones, occur at the unconformity between sandstone and basement rocks beneath 700 m of sandstone. The structurally-controlled mineralization occurs along the Saskatoon Lake electromagnetic Conductor (SLC), which follows the graphitic metasedimentary basement unit (Rippert *et al.*, 2000; Lorilleux *et al.*, 2003). It corresponds to a ~80 m wide, graphite-rich, basement-rooted reverse fault zone, which offsets the unconformity and attenuates in the sandstone cover. The ore bodies are associated with breccia zones developed along a series of shallow-dipping reverse faults that intersect the SLC and have produced fault wedges at the unconformity (Lorilleux *et al*., 2002). The greatest mineralized width reaches 100 m and the maximum grade intersected in drill core is 6.14% U over 10.1 m (She 87). The relatively massive pitchblende mineralization occurs in the sandstone at, and up to 20 m above, the unconformity and, to a lesser extent, as narrow veins in the basement rocks extending to 40 m below the unconformity.

ANALYTICAL METHODS

Petrographic data were obtained from observations of polished thin-sections using an Olympus BH2 polarizing microscope and from examination of freshly-fractured and gold-coated rock chips using a JEOL JSM5600LV scanning electron microscope (SEM) equipped with an energy dispersive spectrometer (EDS) using a Si(Li) semi-conductor detector. Analytical conditions included an accelerating voltage of 15 kV, a probe current of 0.66 nA, and a working distance of 20 mm.

Table 1. Lithostratigraphy of the Athabasca Basin (after Ramaekers *et al*., 2001).

Formation	Abbreviation	Lithology
Otherside	OS	Fine-grained sandstone with granular pebbles
Locker Lake	LL	Fine- to coarse-grained pebbly sandstone; minor thin siltstone and mudstone beds
Wolverine Point B	WPb	Very fine- to medium-grained sandstone interbedded with siltstone and mudstone
Wolverine Point A	WPa	Very fine- to coarse-grained sandstone; minor thin siltstone and mudstone beds
Lazenby Lake	LzL	Thin basal conglomerate; fine- to coarse-grained pebbly sandstone
Manitou Falls D	MFd	Fine- to coarse-grained and pebbly sandstone
Manitou Falls C	MFc	Basal conglomerate; medium- to coarse-grained and pebbly sandstone

Electron microprobe analyses (EMPA) for Na, Mg, Al, Si, Mn, Fe, Ti, K and Ca were performed using a CAMECA SX50 instrument equipped with a wavelength dispersive spectrometer (WDS). The microprobe was calibrated using synthetic and natural oxides and silicates ($MnTiO_3$, hematite, albite, orthoclase and diopside) and corrections were made using a ZAF program. The analytical conditions included a current of 4 nA, an accelerating voltage of 15 kV, a spot size of 2 μm, and a counting time of 10 s per element. The relative errors on the analyzed values are <1.5%. Total Fe is presented as Fe_2O_3.

The sandstone core samples were disaggregated using a freeze-thaw technique (Liewig *et al.*, 1987). This methodology was chosen over the classical grinding method to minimize contamination of the clay-size fraction with fine-grained shards of detrital and over-growth quartz and coarse-grained detrital mica that are created by the grinding process. The disaggregated material was then shaken mechanically in water for 12 h to liberate the clay-size particles. The different clay-size fractions (<2 μm, 1−2 μm, 0.2−1 μm, <0.2 μm) were separated by centrifugation without chemical pre-treatment (Moore and Reynolds, 1989) using a Jouan GR4.22 centrifuge (<2 μm and <1 μm fractions) and a Beckman J2 21 ultra-centrifuge (<0.2 μm fraction).

Grain-size distribution measurements of clay-size samples were carried out using the Mastersizer IP laser particle sizer (Malvern Instruments Ltd.). A 45 mm lens was used for the experiments corresponding to a size range from 0.1 to 80 μm. Clay-size samples were first suspended in deionized water and then ultrasonic dispersion was used in order to achieve disaggregation. The suspensions were then gently poured into the fluid module of the granulometer and measurements were made on three replicates.

X-ray diffraction (XRD) analyses were performed on a SIEMENS D501 diffractometer using CuKα radiation at 1.6 kVA (40 kV and 40 mA), a Si(Li) detector, and divergence slit, receiving slit, and scatter slit at 1º, 0.1 mm and 1º, respectively. Oriented clay mounts were prepared using a slurry method and were analyzed under air-dried (AD) conditions and after ethylene glycol (EG) solvation. Relative humidity was not controlled. The EG solvation was performed using liquid EG as a spray. The XRD patterns were recorded from 2.5 to 33º2θ (40−3 Å) with a step size of 0.02º2θ and a counting time of 4 s per step. *Diffract-AT* software (SOCABIM) was used for background stripping, indexing of the diffraction peaks,

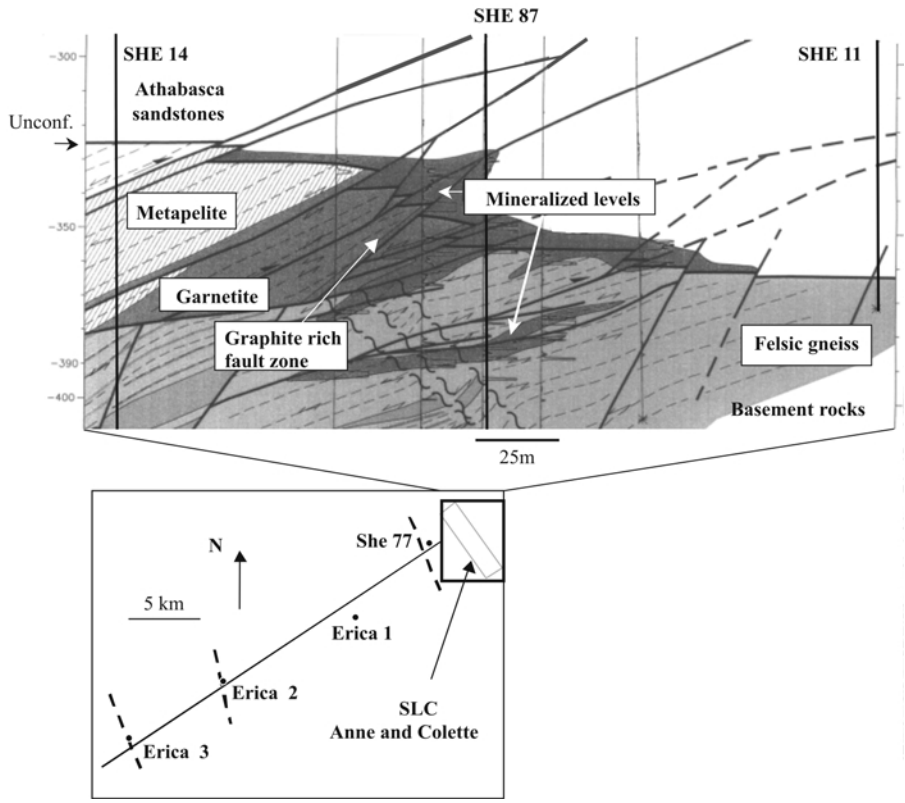

Figure 2. Drill-hole distribution in the Erica-Shea Creek region, with the dashed lines representing graphite-bearing basement structures. The main structure is the SLC (Saskatoon Lake Conductor). The location of the mineralized zones, as well as the main basement structures, are presented in detail for the Anne mineralized area. Unconf.: sub-Athabasca unconformity.

and mineral identification by comparison with the International Centre for Diffraction Data files.

Illite polytypes were identified by XRD analyses on clay-sized material that was randomly oriented using a back-loading method (Moore and Reynolds, 1989). The XRD patterns were recorded from 19 to 34°2θ (4.67−2.64 Å) with a step size of 0.02°2θ and a counting time of 10 s per step. Illite polytype identification was based on comparisons with reference data for $2M_1$ polytypes (Bailey, 1980; Brindley, 1980) and for pure *tv*-1*M* and *cv*-1*M* polytypes (1*M* polytype with vacancy in *trans*- and *cis*-sites, respectively – Drits *et al*., 1993). Note that earlier workers used the terms '1*M*' and '3*T*' for illite polytypes that are now considered to be *tv*-1*M* and *cv*-1*M* (Drits *et al.*, 1993; Reynolds, 1993).

To assess the possible presence of interstratification of *cis*-vacant (*cv*) and *trans*-vacant (*tv*) layers, the *d* values of illite 112 reflections were obtained using elementary Gaussian deconvolution of the XRD patterns (*DecompXR* software; Lanson, 1997) and were compared to literature data (Drits and McCarty, 1996).

SAMPLING

149 core samples were collected from six vertical diamond drill holes (Figure 2). Three drill holes (Erica 1, Erica 3, She 77) were selected from a regional transect perpendicular to the SLC structure, which hosts the Shea Creek U mineralization. Two of these drill holes (Erica 3, She 77) intersected basement graphitic conductors striking subparallel to the SLC and encountered altered zones on both sides of the unconformity. Minor U enrichment was detected near the unconformity in drill hole Erica 3. Located ~7 km southwest of the Shea Creek mineralization, Erica 1 is the only drill hole that did not intersect a graphitic conductor in the basement or any significant alteration. Two other unmineralized drill holes (She 14, She 11), located 100 m west and east of the Anne ore body, respectively, intersect the Shea Creek host-rock alteration halo. Another drill hole (She 87) intersects the Anne ore body (6.14% U over 10.1 m) and the inner part of the host-rock alteration halo on both sides of the unconformity. Both sandstone and basement samples were collected from each drill hole at varying distances from the unconformity and any U anomalies.

RESULTS

Regional sandstone mineralogy and petrography

Diagenetic processes related to burial have been observed in all the sandstone samples from the study area, but are most evident in samples from drill hole Erica 1 which were unaffected by alteration related to U mineralization. In thin-section, the presence of concavo-convex mutual grain contacts between detrital quartz grains, quartz overgrowth triple-point junctions, and horizontal, bedding-parallel stylolite joints (characterized by deformed and compressed coarse-grained detrital micas) attest to the burial compaction undergone by the sandstones. Pressure-solution features and associated syncompactional secondary quartz overgrowths are widespread (Figure 3a) and are especially abundant in the clay-poor (<3%; Kister *et al*., 2006, this issue) quartz-cemented sandstones from the upper formations (OS, LL, WPb, WPa). In the lower formations, secondary quartz overgrowths are scarce (LzL, MFd) to absent (MFc) and quartz grains appear to 'float' in a clay matrix (Figure 3b).

Early hematite is common as pore-filling material (specular hematite) and as a fine-grained dusty coating at the boundary between the secondary quartz overgrowths and the underlying detrital quartz (Figure 3a).

Two authigenic clay minerals were observed in the sandstones (Table 2): (1) coarse-grained minerals of the kaolin sub-group ('kaolin'), and (2) illite. As is generally observed in the Athabasca Group (Quirt, 2003), the diagenetic clay mineral assemblage is dominated by kaolin. Illitization of kaolin is relatively weak and as the illitization process did not go to completion (cf. Hoeve and Quirt, 1984), kaolin still remains in the pore space.

The size of the kaolin crystals typically exceeds 2 μm, thus the <2 μm clay-size fraction used in the present study (Table 2) does not include these coarser mineral grains. Kister *et al*. (2006, this issue) presents the calculated whole-rock normative clay mineral proportions.

The habit of the kaolin is variable, ranging from a vermicular arrangement of pseudohexagonal plates (Figure 3c) typical of kaolinite to a blocky habit typical of dickite (Ehrenberg *et al.*, 1993; Beaufort *et al.*, 1998). Kaolin occurs as pore-filling cement and rarely as replacement of detrital micas in all the sandstone formations. Illite crystals occur as radial intergrowths into open pore space (Figure 3d), as replacements of kaolin (Figure 3c) and of detrital micas, the latter being generally preserved.

Petrography and mineralogy of the altered host rock

Host-rock alterations have affected the sandstone and basement rocks on both sides of the unconformity. Typical alteration features include bleaching (loss of diagenetic hematite), quartz dissolution, illitization, chloritization, phosphatization, and local tourmalinization (Hoeve and Quirt, 1984, 1987; Laverret, 2002). Quartz dissolution has locally led to loss of coherence and collapse of the sandstone (Lorilleux *et al.*, 2002). The intensity of the alteration features and the nature and relative amount of the secondary minerals change with distance from the U ore bodies and related structural features (faults, fractures, breccias).

Alteration in the Athabasca sandstones

In the Anne Zone, a clay mineral alteration halo extends in the Athabasca sandstone from a few tens of meters to several hundred meters above the unconfor-

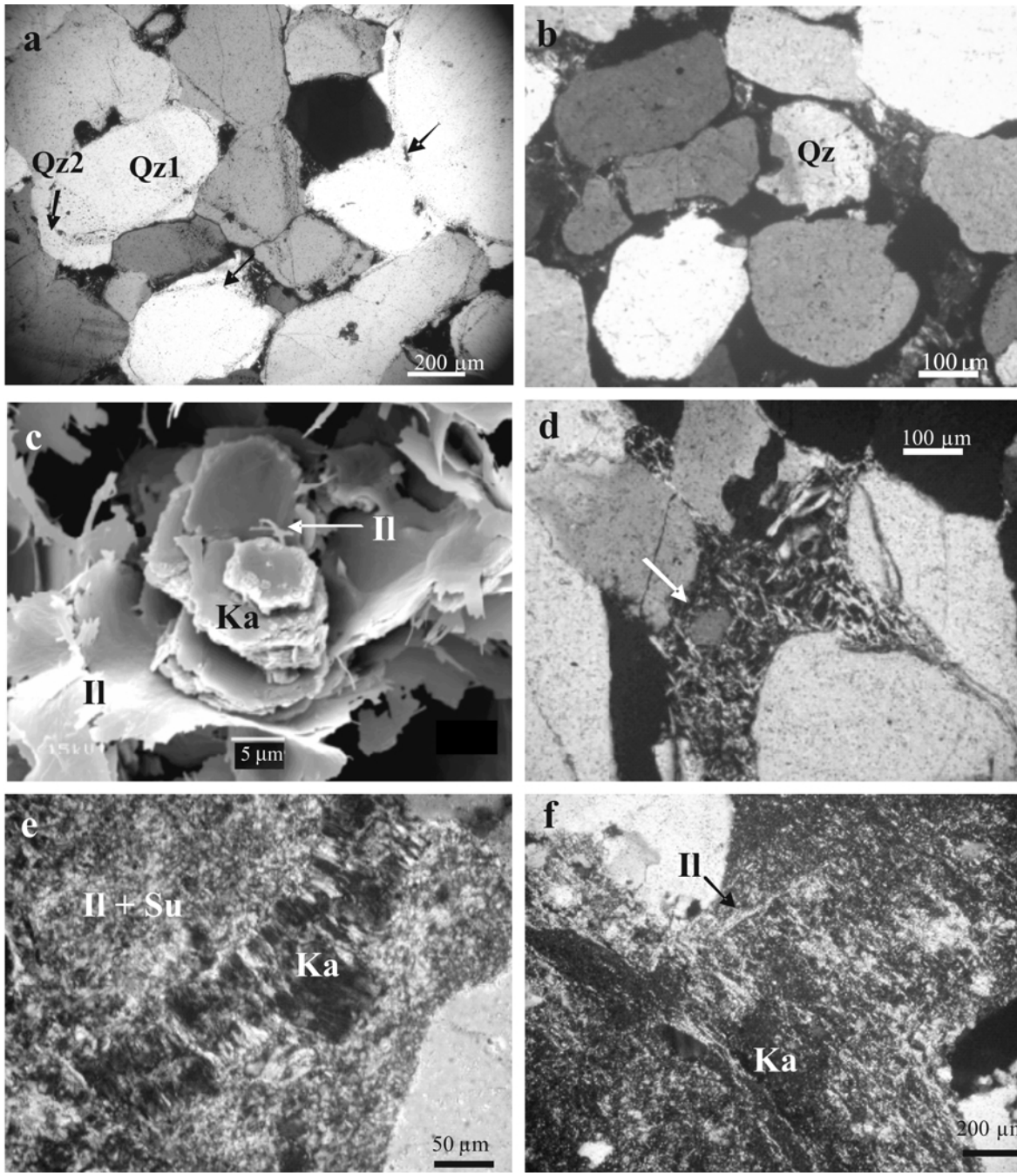

Figure 3. Photomicrographs depicting petrographic features of Athabasca sandstone and sub-Athabasca regolith. (a) Highly silicified sandstone in which quartz overgrowths (Qz2) occupy all the pore space. Detrital grain (Qz1) boundaries are marked by minor amounts of dusty hematite (arrows). Erica 1, 113.3 m, LL formation. (b) Quartz grains (Qz) floating in hematitic clay matrix. Erica 1, 790.3 m, MFc formation. (c) Vermicular habit kaolinite (Ka) partly replaced by lath-like illite (Il). Erica 1, 790.3 m, MFc formation. (d) Illitic matrix crystallized in pore space between quartz grains. Some quartz grains display dissolution embayments (arrow). Erica 1, 598.5 m, LzL formation. (e) Illite + sudoite (Il+Su) replacing kaolin (Ka). She14, 706.2 m, MFc formation. (f) Illite (Il) and kaolinite (Ka) in the sub-Athabasca regolith. Erica 1, 803.1 m.

mity. The intensity of the alteration features increases towards the U mineralization. Alteration is particularly intense in the basal MFc formation and around faults and breccias, and is characterized by concomitant and significant decrease in the abundance of kaolin and increase in the amount of clay minerals (illite and sudoite), the latter mainly due to intense dissolution of detrital quartz as shown by petrographic studies and

mass-balance calculations (Hoeve and Quirt, 1984; Lorilleux *et al.*, 2002).

In the outer alteration halo of the Anne Zone, illite is the only clay mineral species in the <2 μm clay-size fraction (She 14, She 11, She 87). It is also the main clay mineral species in the barren alteration zones intersected by the two drill holes which crosscut basement graphitic conductors striking subparallel to the SLC (Erica 3 and She 77). Illite forms a very fine-grained matrix which replaced the earlier clay mineral assemblage of kaolin and disseminated coarser-grained illite. An intimate mixture of very fine-grained illite and sudoite (di,trioctahedral chlorite) constitutes the clay mineral assemblage (Figure 3e) of the inner alteration zone which is restricted to the MFc and, locally, MFd formations (Kister *et al.*, 2006, this issue). It replaces the earlier clay mineral assemblage.

Acicular dravite and minor amounts of APS are associated with both the illite and the illite + sudoite assemblages.

Alteration in the basement rocks

In the vicinity of the graphite-rich fault zone (Figure 2), the basement rocks have been strongly affected by alteration related to U mineralization (drill hole She 87) and all the pre-existing minerals have been extensively corroded, dissolved, and/or replaced by a clay mineral assemblage composed of variable amounts of illite, sudoite, trioctahedral chlorite, and APS minerals. Close to the unconformity, the altered rocks now consist of massive clay and the presence of the regolith zone is only suggested by minor relict kaolinite (Figure 3f). Distinct changes in clay mineralogy in the basement rocks are observed, with a broad zonation of the dominant clay species from illite to sudoite then to trioctahedral chlorite with increasing distance from the U ore bodies (Hoeve and Quirt, 1984; Laverret, 2002). Alteration in the basement rocks extends up to 100 m below the unconformity.

Illite textures, crystal structure and mineral chemistry

Illite textures. Illite in regional samples, which do not exhibit host-rock alteration features, display predominantly lath-like shapes. Illite crystals have grown from the edges of dickite or kaolinite crystals and commonly occur in sets of laths 120° apart. In the upper formations (LL, OS, WP), illite consists mostly of elongated laths up to 1 μm wide and a few tens of micrometers long (Figure 4a,b,c). At greater depth (MF formation), illite laths are larger (up to 10 μm wide) and appear more rigid, suggesting a concomitant increase in their thickness and the **c*** axis (Figure 4d).

The illite textures seen in the altered sandstones are more heterogeneous. Two main illite habits, the relative proportions of which vary with respect to the distance to the unconformity, are observed by SEM. In the outer alteration halo, very thin 'hairy' illite occurs with dominant coarse-grained lath-like rigid illite particles similar to the 'regional' illites. Hairy illite is abundant in strongly illitized sandstones of the inner alteration halo in the MFc formation and in the lower LzL formation, whereas coarser, lath-like illite dominates the relatively illite-poor, quartz-cemented sandstones of the stratigraphically-higher MFd formation. Mutual contact relationships between the two illites confirm that coarse grained lath-shaped illite formed prior to the hairy illite (Figure 4e,f). When present, fine-grained sudoite is intimately associated with illite.

In altered basement rocks, the illite is intimately associated with both very fine-grained sudoite and Fe-Mg chlorite. The illite in these clay mineral assemblages consists of very fine-grained (sub-micrometer) crystals with mixed lath-like and hairy morphologies. Increasing amounts of illite in the clay mineral assemblages (based on XRD) coincide with SEM observations of increasing amounts of hairy illite.

Illite crystal structure. X-ray diffracttion patterns of oriented preparations of illites confirm the absence of expandable layers, as no changes occur to either the position or peak profile of 00*l* index reflections of illite following EG solvation. The XRD patterns of oriented mounts of illitic material from the altered basement rocks also indicate that most samples contain only illite without expandable layers, but local occurrences of illite-smectite (I-S) mixed-layer clay have been identified. In these samples, the 001 reflection (10.4−10.6 Å under AD conditions) splits into two reflections at 9.7−9.8 Å and 10.7−10.9 Å, respectively, following EG solvation. The proportion of illite in the I-S clay was estimated to be 85% by comparison of the XRD patterns with published Newmod XRD profiles (Reynolds, 1985).

The *hkl* reflections of the various polytypes of illite have been indexed from XRD patterns on randomly oriented powder mounts of bulk clay material (Figures 5, 6). A very small contribution of the $2M_1$ polytype was identified in some samples and has been attributed to the presence of detrital micas as the intensities of the $2M_1$ XRD reflections correlate with the relative abundance of detrital micas observed by petrography.

Both regional and alteration illites are dominantly 1*M* polytypes, but display significant differences in the position of their octahedral vacancy. The degree of interstratification between these different illite structures has been evaluated by comparison of *d* values of illite reflections (derived from Gaussian curves of peak-fitted XRD patterns) with data from Drits and McCarty (1996) as being typical of pure *cv*- and *tv*-1*M* species (Figure 7, Table 3). In such a case, decomposition may be used to determine the respective positions and the relative intensities of the reflections corresponding to the physically different species. The $11\bar{2}$ and $11\bar{3}$ reflections were taken into account for the few samples not

Table 2. Clay mineralogy of the <2 μm fraction of sandstone and basement samples from the Shea Creek region.

Erica 1					Erica 3						She 77					
Depth (m)	Form.	<2 μm clay fraction Chlorite	Illite	Kaolin	Depth (m)	Form.	<2 μm clay fraction Chlorite	Sudoite	Illite	Kaolin	Depth (m)	Form.	<2 μm clay fraction Chlorite	Sudoite	Illite	Kaolin
50.7	OS		XXX	XX	37.2	OS			XXX	XX	34.7	LL			XXX	X
113.3	LL		XXX	XXX	88.1	LL			XXX		86.7	LL			XXX	X
162.6	LL		XXX	X	152.0	LL			XXX		153.7	WPb			XXX	X
232.1	WPb		XXX	(X)	218.4	WPb			XXX	(X)	193.2	WPb			XXX	(X)
303.2	WPb		XXX	XXX	261.7	WPb			XXX	XX	275.1	WPa			XXX	X
359.0	WPa		XX	XXX	330.8	WPa			XXX	X	352.3	WPa			XXX	
417.2	WPa		XX	XXX	406.8	WPa			XXX		447.1	LzL			XXX	
454.2	WPa		XXX	XX	509.0	LzL			XXX	X	516.7	LzL			XXX	XX
511.4	LzL		X	XXX	595.7	LzL			XXX	(X)	604.5	MFd			XXX	
581.0	LzL		XXX	(X)	613.4	LzL			XXX	X	648.8	MFd			XXX	
598.5	LzL		XXX		639.7	MFd			XXX	X	687.8	MFc			XXX	
652.7	MFd		XXX		665.2	MFd			XX	XXX	689.8	MFc			XXX	
710.2	MFd		XX	XXX	668.0	MFd			X	XXX	728.5	MFc				(X)
755.7	MFc		XXX	?	695.1	MFd			X	XXX	738.7	MFc		XX	X	XXX
790.3	MFc		XX	XXX	707.0	MFc			XXX	X	744.4	MFc		X	XXX	X
803.1	Bast		X	XXX	723.7	MFc			XXX	XX	746.1	Bast		X	XXX	XXX
843.5	Bast	X + C-S	XXX		740.8	MFc			XXX	XX	748.0	Bast		X	XXX	XXX
877.1	Bast	XX	XXX		752.2	MFc			XX	XXX	761.9	Bast		XXX	XX±I-S	
					755.4	Bast		XX	XXX	XXX	769.7	Bast		XX	X±I-S	
					764.2	Bast		XXX	XX		780.3	Bast		X	XX±I-S	XXX
					776.7	Bast		XXX	XX±I-S		787.6	Bast		XX	XXX±I-S	XXX
					786.2	Bast		XXX	XX±I-S		792.5	Bast	XXX		XX	(X)
					793.3	Bast	XX		XXX		801.8	Bast	XXX			X
					805.6	Bast		XXX	XX		825.4	Bast	(X)		XXX	
					815.7	Bast		X	XXX							
					845.2	Bast		X	XXX±I-							
					855.7	Bast		X	XXX±I-S							
					858.8	Bast		X	XXX±I-S							
					861.6	Bast		X	XXX±I-S							
					863.4	Bast		X	XXX±I-S							

Table 2 continued

She 11						She 14						She 87					
Depth (m)	Form.	<2 μm clay fraction				Depth (m)	Form.	<2 μm clay fraction				Depth (m)	Form.	<2 μm clay fraction			
		Chlorite	Sudoite	Illite	Kaolin			Chlorite	Sudoite	Illite	Kaolin			Chlorite	Sudoite	Illite	Kaolin
56.0	LL			XXX	(X)	65.4	LL			XXX	X	35.2	LL			XXX	XX
90.9	WPb			XXX	(X)	101.6	WPb			XXX	X	75.2	WPb			XXX	(X)
98.1	WPb			XXX	(X)	126.2	WPb			XXX	X	104.2	WPb			XXX	XX
146.1	WPb			XXX	X	199.8	WPa			XXX	XX	145.1	WPb			XXX	X
205.5	WPa			XXX	X	253.8	WPa			XXX		211.4	WPa			XXX	X
248.8	WPa			XXX		351.4	WPa			XXX		265.0	WPa			XXX	
290.8	WPa			XXX	X	378.0	LzL			XXX		315.8	WPa			XXX	
349.3	WPa			XXX		399.1	LzL			XXX		359.5	LzL			XXX	
407.4	LzL			XXX		443.5	LzL			XXX		404.3	LzL			XXX	
441.7	LzL			XXX		448.8	LzL			XXX		451.4	LzL			XXX	XX
502.2	LzL			XXX		497.3	LzL			XXX		501.0	LzL			XXX	
549.6	LzL			XXX		550.0	MFd		XXX	XXX	XX	548.2	MFd		X	XXX	
606.1	MFd			XXX		599.8	MFd		XXX	X	XXX	600.0	MFd		XXX	XXX	
653.2	MFc			XXX		643.0	MFc	(X)		XXX	X	614.2	MFd		X	XXX	
701.1	MFc		XXX	XX		670.0	MFc		XX	XXX		627.7	MFc			XXX	
717.5	MFc		XXX	(X)		681.0	MFc		XX	(X)	XX	631.5	MFc			XXX	
728.9	MFc		X	XX	XXX	695.1	MFc		XX	(X)	XXX	643.8	MFc			XXX	
729.7	Bast		X	XXX		702.2	MFc		XX	XXX	X	666.1	MFc		X	XXX	(X)
733.4	Bast			X	XXX	706.2	MFc		XX	XXX	(X)	674.2	MFc		XXX	XX	
						707.6	Bast		XXX	X		698.6	MFc		X	(X)	XXX
						710.7	Bast	X	X	X	XXX	704.1	MFc			(X)	X
						733.4	Bast	X		XX±I-S	X	708.3	MFc			(X)	X
						755.0	Bast	XXX		X		711.7	Bast	X	X	X	XXX
						762.0	Bast	XXX		XXX		716.0	Bast		X	XXX	
						774.4	Bast	XXX		XX±I-S		716.5	Bast			XXX	
						780.0	Bast	XXX		XX±I-S	XX	723.5	Bast			XXX	
						787.4	Bast	XXX		X±I-S		727.9	Bast		X	XXX	
												734.2	Bast		XXX	XXX	
												739.9	Bast		(X)	XXX	
												754.6	Bast	XXX		X±I-S	
												770.8	Bast	X		XXX	

XXX, XX, X, (X): decreasing intensity of the diffraction peaks; ?: suspected; C-S: chlorite-smectite mixed-layer minerals; I-S: illite-smectite mixed-layer minerals.

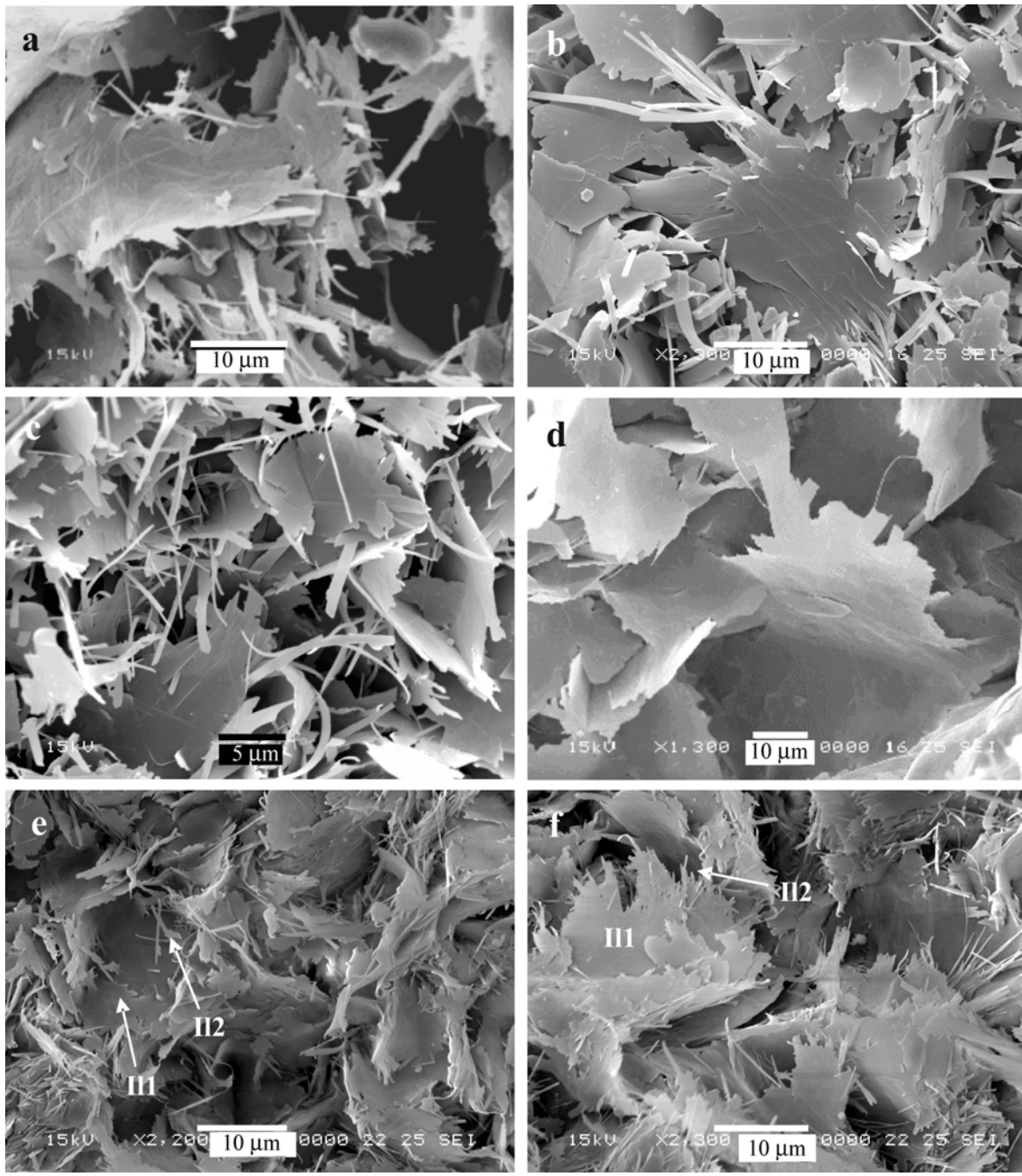

Figure 4. SEM images of illite morphologies. (a) Erica 1, 113.3 m, LL formation. (b) Erica 1, 359 m, WPa formation. (c) She 14, 101.6 m, WPb formation. (d) Erica 1, 755.7 m, MFc formation. (e,f) She 87, 666.1 m, MFc formation. Il1: lath-shaped illite; Il2: hairy illite.

contaminated by $2M_1$ micas, sudoite and kaolin mineral reflections, because of the superimposition of their reflections.

It appears from these data that illite consists of: (1) *cv*-1*M* structures without interstratification with *tv*-1*M* ($d_{112} \approx 3.12$ Å). The layer proportion of *cv*-1*M* type (W_{cv}), deduced from Drits and McCarty (1996), is close to 1. (2) *tv*-1*M* rich structures, the d_{112} values for which (generally ~3.06–3.07 Å), may suggest mixed layering with up to 20% of *cv*-1*M* layers. Greater proportions of *cv*-1*M* layers have been observed in only two samples from the basement rocks crosscut by She 87.

These data do not integrate the influence of the P_0 parameter (probability of zero degree layer rotation).

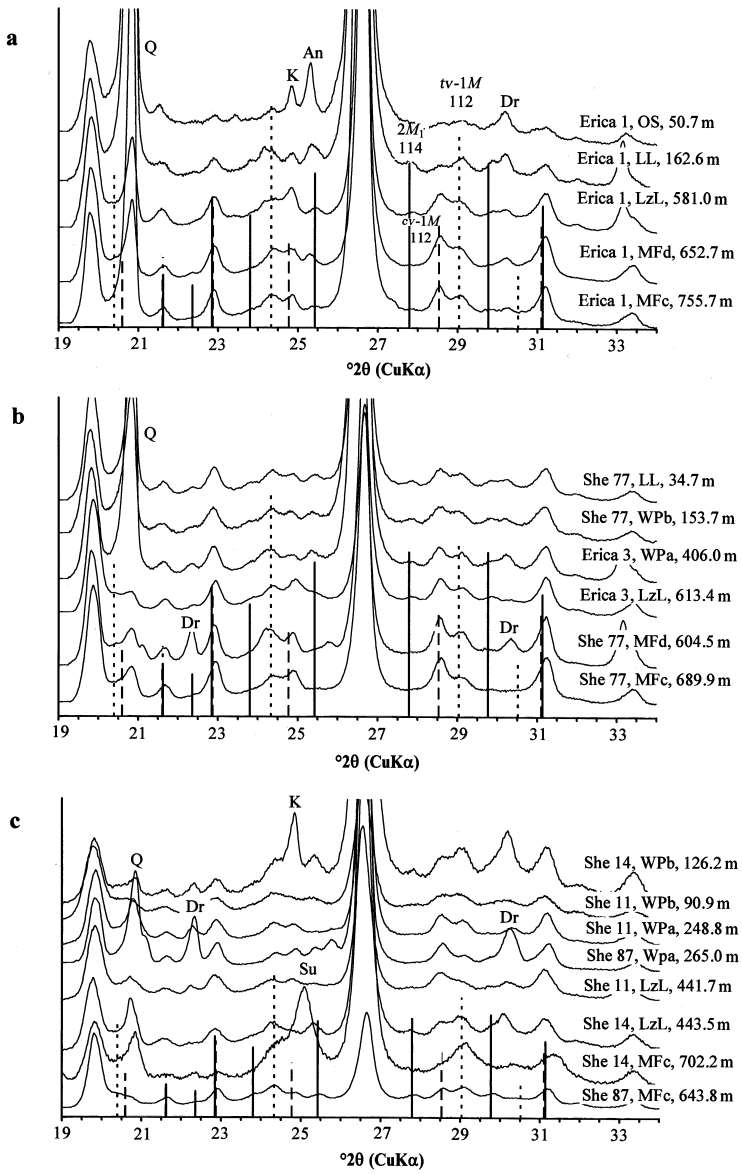

Figure 5. XRD patterns of random powder mounts (<2 μm clay-size fraction) of sandstone samples from (a) drill hole Erica 1, (b) distal drill holes, and (c) Anne area drill holes. The *d* values and relative intensities of $2M_1$, *tv*-1*M*, and *cv*-1*M* illites have been calculated according to the method suggested by Drits *et al.* (1993). Q: quartz; An: anatase; Dr: dravite; K: kaolin; Su: sudoite.

According to Drits and McCarty (1996), W_{cv} values increase with decreasing values of P_0. As an illustration, the layer proportion of type *cv*-1*M*, in some cases >1 (see Table 3), probably results from this kind of defect ($P_0 < 1$). The determination of W_{cv} from the 112 reflection gives generally reliable results since the d_{112} maxima are not very sensitive to either the type or the amount of stacking defaults. A possible explanation for the different *d* values obtained for the 112 reflection of *tv*-1*M* rich varieties is an interlayer displacement that is slighty different from the ideal values determined by Drits *et al.* (1993). However, the $|c.\cos\beta\alpha|$ values of 0.307−0.309 and 0.362−0.369, respectively, for the two families are consistent with *cv*-1*M* structures (W_{cv} > 90%, $|c.\cos\beta\alpha| = 0.400$ for the pure *cv*-1*M* end-member) and with *tv*-1*M*/*cv*-1*M* mixed layers with 20−30 % of *cv*-1*M* layers. For simplification, we will use the terminology *cv*-1*M* and *tv*-1*M* polytypes, respectively, for the two populations of illite identified.

Illite from the regional background is composed of a mixture of both *tv*-1*M* and *cv*-1*M* polytypes with a general trend to an increase in the relative amount of *cv*-1*M* polytype with increasing burial depth (Figure 5a and intensity ratio between the 112 reflections of the *cv*- and *tv*-1*M* rich varieties on Table 3). A similar trend is present in the Erica 3, She 77 and She 11 drill holes which show a weak to moderate overprint by host-rock alteration (Figure 5b,c, Table 3).

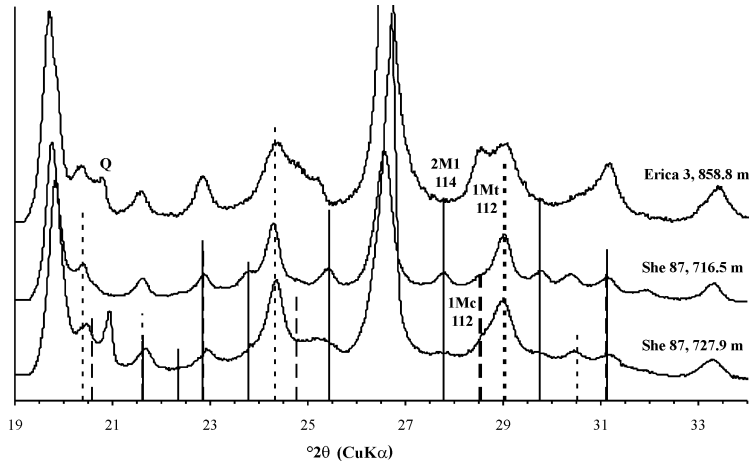

Figure 6. XRD patterns of random powder mounts of altered basement samples. The *d* values and relative intensities of $2M_1$, *tv*-1*M*, and *cv*-1*M* illites have been calculated according to the method suggested by Drits *et al*. (1993). Q: quartz.

Illites from the alteration halo around the Anne ore body show a depth-related reversal of the illite polytype trend relative to the regional illite (Figure 5c, Table 3). In samples from drill holes She 14 and She 87, there is a significant increase in the relative proportion of the *tv*-1*M* polytype (hairy habit) towards the mineralized zone at the unconformity in all clay mineral assemblages (illite, illite + sudoite). In the strongly-altered basement rocks, the illitic material is also a mixture of *tv*-1*M* and *cv*-1*M* polytypes, with dominant *tv*-1*M* polytype (Figure 6). The clay particle size distribution was compared with the 3D crystal structure of the bulk illitic material from sudoite-free samples (drill hole She 87). This comparison (Figure 8) illustrates: (1) the zonation from background sandstone (145.1 m) to altered sandstone (631.5 m) and altered basement rocks (708.6 m); and (2) a general enrichment in *tv*-1*M* illite in the strongly altered rocks located close to the unconformity. The granulometric curves display a bimodal distribution with two modes near 3–6 μm and 0.5 μm and an increase in the amount of *tv*-1M illite which parallels increases in the amount of the fine-grained fraction. The 3D crystal structures of illite from different size fractions demonstrate that the *tv*-1*M*/*cv*-1*M* ratio increases with decreasing grain size (Figure 9).

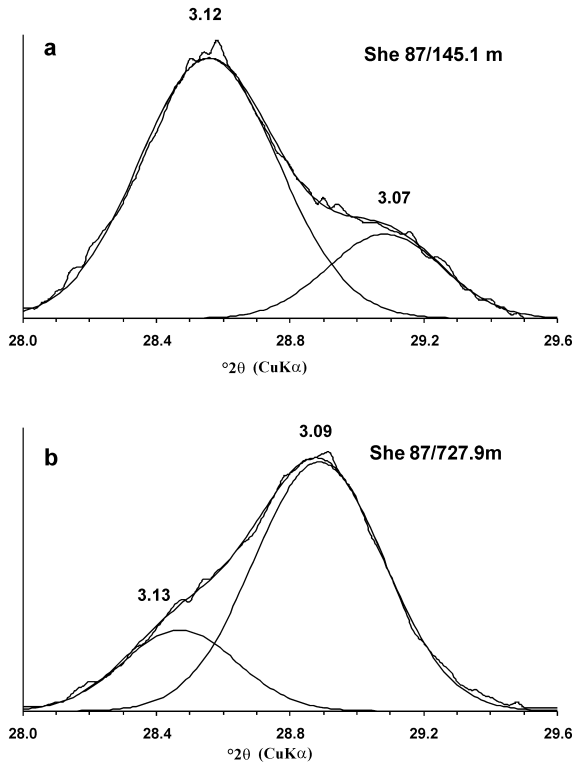

Figure 7. Examples of decomposition of illite 112 XRD reflections with elementary Gaussian curves (DecompXR software; Lanson, 1997). (a) Sample She 87, 145.1 m; (b) sample She 87, 727.9 m.

Illite mineral chemistry. Illite chemical analyses by electron microprobe and calculated structural formulae of illites from regional background rocks, from weakly to strongly altered sandstone, and from altered basement rocks are presented in Table 4. The regional illites include examples from the different sedimentary formations (OS, LL, WPa and MFd). Altered sandstone samples (LzL, MFc) containing mixtures of illite polytypes with different textures were taken from the drill holes that intersected the alteration halo. Samples of illitic altered basement rocks were taken at varying distances from the Anne ore body.

Illites have a very similar composition (Figure 10). They are all aluminous, with a Si content between 6.4 and 6.8 atoms per formula unit (a.p.f.u.) and low Fe and Mg contents (0.04–0.14 a.p.f.u. and 0.10 to 0.30 a.p.f.u., respectively). The interlayer charge is essentially compensated by K^+ cations and ranges between 1.6 and 1.8 a.p.f.u.

Both the coarse-grained, lath-like illites and the hairy illites present in the altered sandstones have chemical

Table 3. *d* values of illite 112 reflections (derived from Gaussian curves of peak-fitted XRD patterns), W_{cv} and |*c*.cosβα| are derived from calculated diffraction patterns and data from Drits and McCarty (1996) as being typical of pure *cv*- and *tv*-1*M* species. The interlayer shift has been calculated using decomposition of the $11\bar{2}$ and $11\bar{3}$ reflections only for samples not contaminated by $2M_1$ micas, sudoite and kaolin mineral reflections, because of the superimposition of their reflections. Ir: intensity ratio between the 112 reflections of the *cv*- and *tv*-1*M* rich varieties.

Drill hole	Depth (m)	Formation	Clay fraction	*cv*-1*M* rich varieties			*tv*-1*M* rich varieties			Ir
				d_{112}	W_{cv}	|c.cosβ/α|	d_{112}	W_{cv}	|c.cosβ/α|	
Erica 1	50.7	OS	<2 μm	3.125	1.1		3.071	0.1		0.8
	162.6	LL	<2 μm	3.120	1.0		3.068	0.0		0.6
	581.0	LzL	<2 μm	3.123	1.1		3.070	0.1		1.6
	652.7	MFd	<2 μm	3.125	1.1	0.308	3.074	0.2	0.369	1.5
	755.7	MFc	<2 μm	3.126	1.2		3.073	0.1		1.5
Erica 3	406.0	WPa	<2 μm	3.124	1.1		3.069	0.1		1.5
	613.4	LzL	<2 μm	3.123	1.1		3.069	0.1		1.8
	858.8	Bast	<2 μm	3.123	1.1		3.071	0.1		0.9
She 77	34.7	LL	<2 μm	3.124	1.1		3.072	0.1		1.4
	153.7	WPb	<2 μm	3.124	1.1		3.074	0.2		1.5
	604.5	MFd	<2 μm	3.124	1.1		3.070	0.1		1.7
	689.9	MFc	<2 μm	3.122	1.1	0.307	3.066	0.0	0.367	2.4
She 11	90.9	WPb	<2 μm	3.119	1.0		3.071	0.1		0.9
	248.8	WPa	<2 μm	3.121	1.0	0.308	3.067	0.0	0.362	1.4
	441.7	LzL	<2 μm	3.118	1.0	0.309	3.072	0.1	0.362	1.8
She 14	443.5	LzL	<2 μm	3.117	1.0		3.067	0.0		0.8
	643.0	MFc	<2 μm	3.124	1.1		3.074	0.2		1.6
	643.0	MFc	1−2 μm	3.123	1.1		3.077	0.2		2.3
	643.0	MFc	0.2-1 μm	3.122	1.1		3.074	0.2		1.6
	643.0	MFc	<0,2 μm	3.123	1.1		3.065	0.0		0.1
	702.2	MFc	<2 μm	3.122	1.1		3.069	0.1		0.2
She 87	145.1	OS	<2 μm	3.125	1.1		3.069	0.1		2.9
	265.0	WPa	<2 μm	3.126	1.1		3.068	0.0		3.1
	631.5	MFc	<2 μm	3.126	1.1		3.073	0.1		1.2
	643.8	MFc	<2 μm	3.126	1.1		3.073	0.1		0.9
	716.5	Bast	<2 μm	3.118	1.0		3.083	0.3		0.2
	727.9	Bast	<2 μm	3.134	1.3		3.090	0.5		0.3

compositions similar to the illites from the regional samples. The only exceptions are in samples from drill hole Erica 3 in which the illites contain a slightly greater Mg content (0.31−0.44 a.p.f.u.). The illites from the altered basement rocks also have compositions similar to those from the sandstone.

DISCUSSION

In the Athabasca Basin, a structural control on both the illitization and U mineralization processes by major faults has been postulated for the eastern Athabasca deposits (Hoeve and Quirt, 1984, among others) and in the Shea Creek region in the western Athabasca (Rippert *et al*., 2000).

The main difficulty in the use of illite as an indicator of host-rock alteration processes in the Athabasca sandstones is differentiating between regional and alteration illites. The Kübler illite crystallinity index (Kübler, 1964), related to the illite 001 full width at maximum value (FWHM), from <5 μm clay-size extracts has been commonly used as an indicator of host-rock alteration processes in the Athabasca sandstone and was identified as a potential exploration vector for unconformity-type U deposits (Hoeve *et al*., 1981; Hoeve and Quirt, 1984). However, the polygenic origin of the illite in the bulk sample hampers a proper distinction between regional and alteration illites. (Table 5).

Both of the illites from sandstone are of the 1*M* polytype with variable proportions of the *tv*-1*M* and *cv*-1*M* varieties. The XRD *hkl* reflections of the $2M_1$ polytype are absent in the <2 μm clay-size fraction of most of the studied sandstones. These results differ from those of Hoeve and Quirt (1984), Ey *et al.* (1985), and Halter (1988) who reported $2M_1$ and 1*M* illites in the Athabasca Basin. The difference can be explained by the smaller size-fraction studied in this work (<2 μm) than that investigated by those authors (<5 μm), as the 2−5 μm size-fraction represents only a small part of the authigenic illitic material, as observed by SEM, and may be contaminated by detrital $2M_1$ micas which are typically >2 μm in size.

However, differences in textural (size, morphology) and structural characteristics (*tv*-1*M*/*cv*-1*M* polytypic

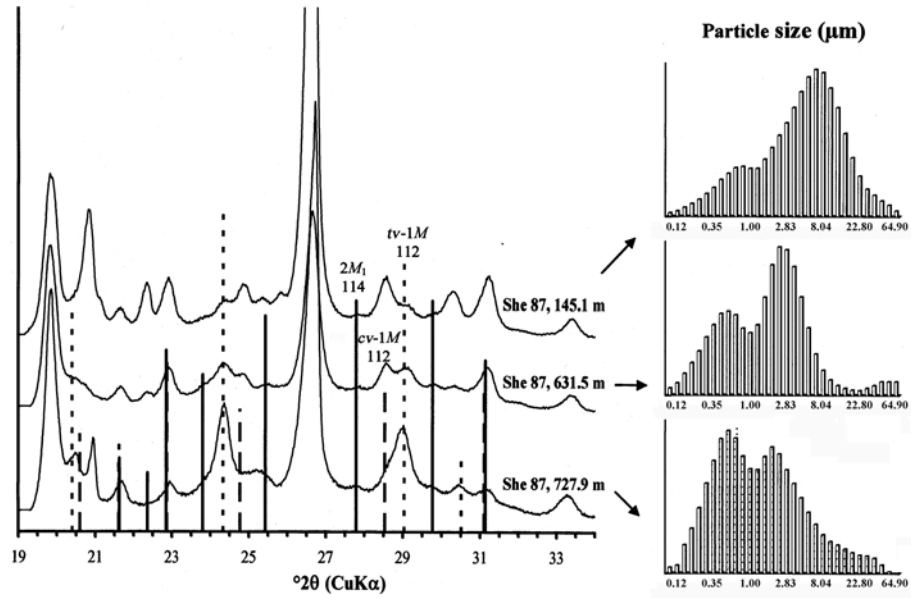

Figure 8. Granulometric curves of bulk clay material from samples She 87, 145.1 m, She 87, 631.5 m, and She 87, 727.9 m. All curves display a bimodal distribution. Increasing amounts of *tv*-1*M* illite coincide with increases in the amount of finer-grained material.

ratio) are observed. The regional illite crystals are relatively coarse grained, lath-like, and dominantly of the *cv*-1*M* polytype, whereas sandstone and basement alteration illite consists of fine-grained hairy crystals dominantly of the *tv*-1*M* polytype.

Regional illites present a marked depth-related evolution of their textural and microstructural characteristics (Erica 1 drill hole: Figures 4a,b,c, 6a). With increasing burial depth, there is: (1) an increase in illite particle size in the *a*-*b* plane, (2) a progressive change from lath-like crystal habits towards more isometric morphology, and (3) an increase in the *cv*-1*M*/*tv*-1*M* polytype ratio. Similar depth-related evolutions of both illite morphology and 3-D illite crystal structure have been described in the burial diagenesis of sandstone basin worldwide (e.g. Reynolds, 1993; Lanson *et al*., 1996, 2002) with burial depths and temperatures similar to those estimated for the Athabasca Basin (5 km and 180ºC, respectively; Pagel, 1975; Hoeve and Quirt, 1984; Derome *et al*., 2003).

Although difficult to characterize because of their mixing with coarse-grained diagenetic illite, it is clear that the illites in the altered sandstones have a smaller size, a predominant hairy habit and a much lower *cv*-1*M*/

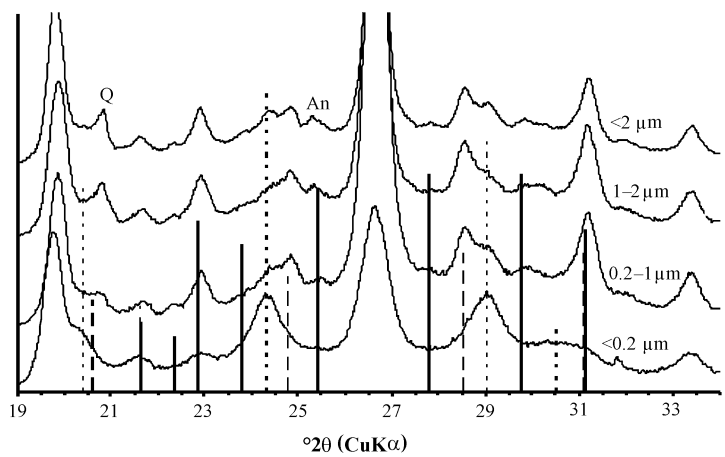

Figure 9. XRD patterns of random powder mounts of various clay-size fractions from sample She 14, 643.0 m. The *d* values and relative intensities of $2M_1$, *tv*-1*M*, and *cv*-1*M* illite XRD reflections have been calculated following the method suggested by Drits *et al*. (1993). Q: quartz, An: anatase. The coarsest size-fraction (1–2 µm) is essentially composed of *cv*-1*M* illite, while the finest size-fraction (<0.2 µm) is essentially composed of *tv*-1*M* illite. Intermediate proportions of each polytype are found in the intermediate size-fractions.

Table 4. Chemical compositions, with standard deviations, of illites from the Shea Creek region. Total oxide percent normalized to 100; structural formula is calculated per $O_{20}(OH)_4$; total Fe expressed as Fe^{3+}; *N*: number of measurements.

	Sandstone								Basement					
Drill hole	Erica 1		She 77		She 87		Erica 3		She 11		She 14		She 87	
N	43		26		48		65		40		25		53	
SiO_2	52.88	0.79	52.84	1.27	52.38	1.41	53.00	1.18	52.52	0.58	52.50	0.58	51.24	0.88
TiO_2	0.05	0.08	0.12	0.14	0.13	0.18	0.05	0.06	0.05	0.06	0.05	0.06	0.04	0.04
Al_2O_3	34.66	1.01	35.24	1.11	35.60	1.16	34.33	1.46	35.31	0.55	35.41	0.57	36.16	0.71
Fe_2O_3	0.95	0.22	0.92	0.14	0.84	0.24	0.93	0.24	0.92	0.22	0.59	0.16	0.99	0.19
MnO	0.06	0.07	0.07	0.11	0.07	0.10	0.04	0.07	0.06	0.08	0.06	0.08	0.04	0.06
MgO	1.04	0.33	0.74	0.17	0.77	0.24	1.18	0.51	0.82	0.10	1.20	0.18	0.80	0.20
CaO	0.16	0.12	0.10	0.11	0.10	0.08	0.10	0.13	0.06	0.06	0.09	0.05	0.07	0.06
Na_2O	0.08	0.06	0.08	0.06	0.06	0.05	0.07	0.13	0.13	0.05	0.12	0.11	0.12	0.05
K_2O	10.12	0.36	9.90	0.55	10.05	0.58	10.30	0.59	10.13	0.27	9.98	0.23	10.54	0.38
Si	6.59	0.09	6.57	0.13	6.52	0.14	6.61	0.13	6.55	0.06	6.53	0.06	6.41	0.09
^{IV}Al	1.41	0.09	1.43	0.13	1.48	0.14	1.39	0.13	1.45	0.06	1.47	0.06	1.59	0.09
^{VI}Al	3.68	0.08	3.74	0.06	3.75	0.06	3.66	0.10	3.73	0.03	3.73	0.04	3.75	0.03
Ti	0.00	0.01	0.01	0.01	0.01	0.02	0.00	0.01	0.00	0.01	0.00	0.01	0.00	0.01
Fe^{3+}	0.09	0.02	0.09	0.01	0.08	0.02	0.08	0.02	0.09	0.02	0.06	0.01	0.09	0.02
Mn	0.01	0.01	0.01	0.01	0.01	0.01	0.00	0.01	0.01	0.01	0.01	0.01	0.00	0.01
Mg	0.19	0.06	0.14	0.03	0.14	0.04	0.22	0.09	0.15	0.02	0.22	0.03	0.15	0.04
Oct. occupancy	3.98	0.02	3.98	0.03	3.99	0.02	3.97	0.02	3.98	0.02	4.02	0.03	3.99	0.02
Ca	0.02	0.02	0.01	0.01	0.01	0.01	0.01	0.02	0.01	0.01	0.01	0.01	0.01	0.01
Na	0.02	0.01	0.02	0.02	0.01	0.01	0.02	0.03	0.03	0.01	0.03	0.03	0.03	0.01
K	1.61	0.06	1.57	0.09	1.60	0.10	1.64	0.10	1.61	0.05	1.58	0.04	1.68	0.07
Int. charge	1.67	0.06	1.62	0.09	1.64	0.10	1.69	0.09	1.66	0.05	1.64	0.05	1.73	0.06

tv-1*M* polytype ratio. Contrary to that observed for regional sandstone, no depth-related variation can be demonstrated for altered sandstone. In both the altered sandstone and the basement rocks, the spatial variations in the *cv*-1*M*/*tv*-1*M* polytype ratio for the illites are structurally controlled. Lower *cv*-1*M*/*tv*-1*M* ratios were

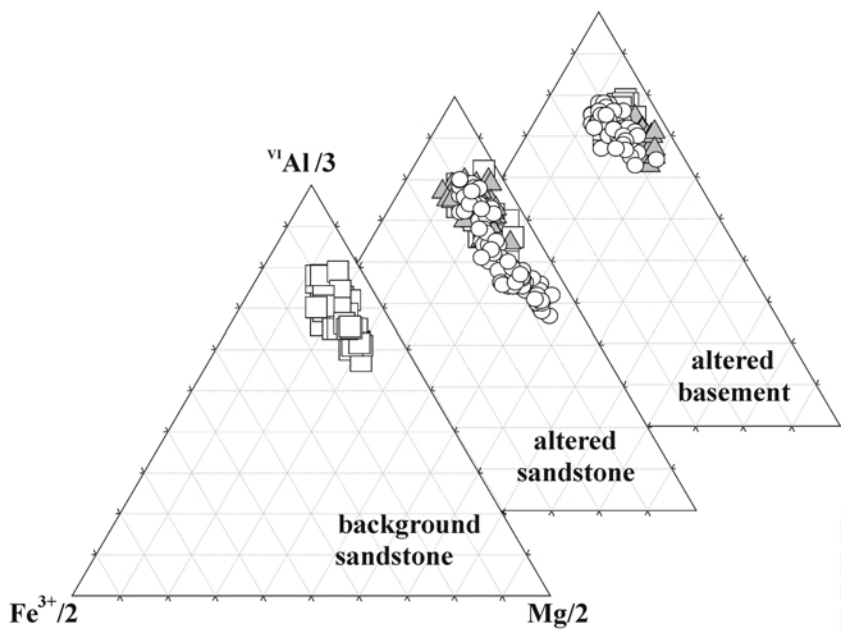

Figure 10. Octahedral cationic composition of illite projected in $^{VI}Al/3-Fe^{3+}/2-Mg/2$ space. Unaltered sandstone samples: Erica 1 drill hole (white squares). Altered sandstone samples: She 77 drill hole (white squares); She 87 drill hole (gray triangles); Erica 3 (white circles). Altered basement samples: She 11 drill hole (white squares); She 14 drill hole (gray triangles); She 87 drill hole (white circles).

Table 5. Comparison of illite characteristics from regional sandstone and from the Shea Creek alteration halo.

Illite type	Paragenesis	Texture	Average width	Morphology	Polytype	Chemistry
Barren area	Illite + hematite ± APS	Pore filling and grain coating Partial replacement of dickite and kaolinite	1−2 μm Depth-related increase of the average width	Mostly lath-shaped Minor amounts of smaller fibrous crystals	Mixture of *tv*-1*M* and *cv*-1*M* (*cv*-1*M* predominant) Depth-related increase of the relative proportion of *cv*-1*M* polytype	Al-rich illite
Alteration halo	Illite + APS ± dravite	Sandstones Pore filling and grain coating				
	Illite + sudoite + dravite + APS	Significant to total replacement of dickite and kaolinite Growth from the edge of coarse grained illites	<0.3 μm	Mostly 'hairy'	Mixture of *tv*-1*M* and *cv*-1*M* (richer in *tv*-1*M*) Increasing of the relative proportion of *tv*-1*M* near the unconformity	Sandstones Al-rich illite
	Illite + tri-tri-chlorite ± sudoite + APS	Basement rocks Significant replacement of alkali feldspars and biotites				Basement rocks Al-rich illite

obtained from samples, located close to the structure hosting the U ore bodies, that contain significant amounts of hairy illite. These samples are located near the unconformity, around fractures in fault-damaged zones, or in porous sandstone horizons which may represent aquifers that were connected to the permeable network controlling the fluid transport during the hydrothermal events. Increases in the proportion of the *tv*-1*M* polytype are particularly marked close to the unconformity in both the overlying MFc formation and the underlying fractured basement rocks. These nearly pure *tv*-1*M* illites are in the inner alteration zone and are often, but not exclusively, associated with sudoite.

Towards a model for illitization in the Shea Creek deposit

In the Shea Creek area, an illitization model consistent with our data and observations deals with two major illitization processes that have affected the sandstones and basement rocks (Figure 11).

First, regional illitization of the Athabasca sandstones took place under conditions of deep burial and consists of variable, relatively weak replacement of detrital and early-diagenetic kaolin (now mostly dickite). This process has been observed on a basinal scale in the Athabasca Basin (Hoeve and Quirt, 1984) and the Kombolgie Basin (Patrier *et al.*, 2003), and it is a common process in the diagenesis of sandstone successions containing reactive K-bearing minerals (*e.g.* K-feldspars) or subjected to invasion by K-bearing solutions (Środoń and Eberl, 1984; Bjorlykke and Aagaard, 1992; Ehrenberg *et al.*, 1993; Berger *et al.*, 1997; Lanson *et al.*, 1996, 2002). In the Athabasca Basin, the source of the K involved in illitization remains unclear because no relict K-feldspar remains.

Partially altered detrital K-mica is the only detrital K-bearing mineral observed in these sandstones and the overall low degree of illitization of kaolin (Hoeve and Quirt, 1984; Laverret, 2002; Kister *et al.*, 2006, this issue) indicates that, whatever the source, the K content of the Athabasca diagenetic brines was small.

Secondly, illitization in host-rock alteration haloes is associated with sandstone-hosted, unconformity-type U deposits in the Athabasca Basin. The current model proposed for the genesis of sandstone-hosted unconformity-type uranium deposits involves a mixing of two brines, one a sodic Athabasca Group formational brine and one basement fluid emerging (egressing) from the basement along faults cutting the sub-Athabasca unconformity (diagenetic-hydrothermal model: Hoeve and Sibbald, 1978; Hoeve and Quirt, 1984; Kotzer and Kyser, 1995; Quirt, 1997; Cuney *et al.*, 2003; Derome *et al.*, 2003). The origin of the basement fluid has recently been postulated to be by infiltration of the diagenetic sodic brines from the basin into the basement, the brine becoming calcic through Ca-Na exchange (due to the albitization of plagioclase in basement rocks), and

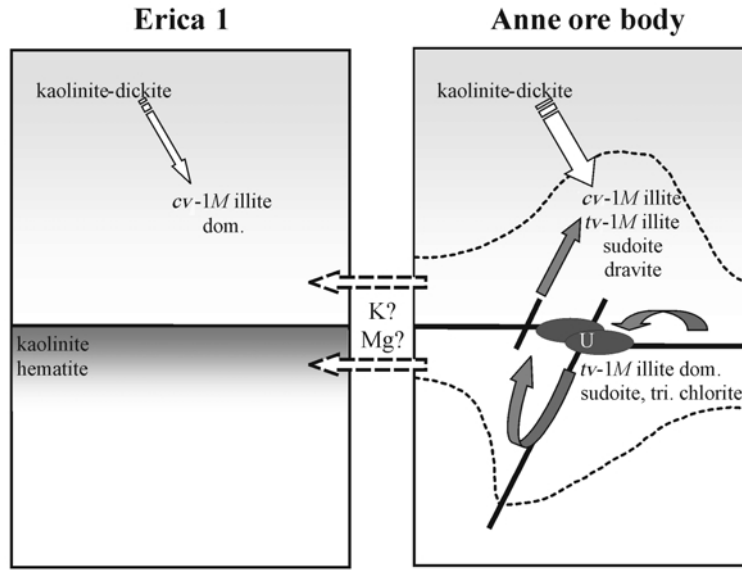

Figure 11. Schematic sketch depicting the illitization processes at the Shea Creek deposit. The 'Erica 1' panel illustrates the diagenetic alteration process; the 'Anne ore body' panel illustrates the basement-sandstone diagenetic-hydrothermal alteration related to U mineralization.

subsequent emergence as a basement fluid into the basin along the graphitic fault (Cuney *et al.*, 2003; Derome *et al.*, 2003). The basement rocks were strongly altered by the infiltrating brine with destabilization of K-bearing silicate minerals (K-feldspar and biotite), their replacement by illite + chlorite assemblages, and the release of the excess K into fluids which, in turn, were progressively neutralized (Raffensperger and Garven, 1995; Komninou and Sverjensky, 1996) and recycled as basement fluid into the overlying basin through tectonic movements (Hoeve and Quirt, 1984; Lorilleux *et al.*, 2002). The influx of K-bearing fluids derived from alteration of underlying basement rocks in turn resulted in illitization of the kaolin present in the volume of sandstone that was infiltrated by these fluids. The degree of illitization of such altered rocks is then related to the K content of these fluids and to the transport conditions of the resulting fluids from basement to sandstone and in the sandstone. The same fluid evolution and host-rock alteration process resulted in the Mg source and transport necessary for the formation of sudoite in the alteration halo and in the basal sandstone along the unconformity (Kister *et al.*, 2006, this issue).

This illitization model accounts for the observed overall chemical homogeneity of the various illites and their observed textural and structural heterogeneities. The chemical homogeneity resulted from the occurrence of a common source for the fluid involved in the illitization process at nearly constant temperature, controlled by the deep burial diagenetic conditions (absence of interstratifications with expandable layers). The model explains that in the absence of faulting and/or alteration of the basement rocks (*e.g.* Erica 1 drill hole), the K needed for the illitization was obtained only through destabilization of minor K-bearing detrital silicates present in the sandstones or through distal migration of K into the diagenetic aquifer from fault zones subjected to basement-sandstone illitization processes. These alternatives suggest that a common source of K may be considered for both the regional barren area and altered sandstone illitization processes. The absence of any Mg-Fe variation in illite composition suggests that illite chemistry was buffered by the associated secondary minerals (mainly sudoite, trioctahedral chlorite and dravite).

The heterogeneity of the mineralogical and geochemical composition of the basement rocks and the expected heterogeneity of the chemistry of the fluid produced by interaction of the basinal brines with such rocks is just perceptible on the relative proportion of the secondary phases (see Kister *et al.*, 2006, this issue).

In a same drill hole, the different polytypes of illite (*tv*-1*M* and *cv*-1*M* polytypes) give a similar range of K-Ar values (Laverret, 2002; Laverret *et al.*, 2003). So, the structural and textural differences observed between illites resulted from their conditions of nucleation/growth. Illite from altered sandstone differs from regional illite by having crystals with smaller size and a fibrous morphology (hairy illite), coupled with a predominant *tv*-1*M* polytype. The occurrences of fibrous illite are poorly understood. Güven *et al.* (1980) and Güven (2001) indicate that the illite fibers have a dioctahedral 1*M* mica structure with *trans*-octahedral vacancies (*tv*-1*M* polytype) and are elongated parallel to the *a* crystallographic axis. Champion (1989), Lanson *et al.* (1996), and Güven (2001) suggest that the fibrous characteristic of illites is symptomatic of crystallization under metastable conditions.

Hydrothermal systems are characterized by highly variable water/rock ratios, durations of water/rock interaction processes, chemical activities in solutions, and flow regimes in response to tectonic activities. They are well known to represent the best candidates for the promotion of explosive nucleation and metastable growth of clay minerals (Clauer and Chaudhuri, 1995; Frey and Robinson, 1999; among others). The variations of textural and structural characters of illite, documented in the fault- and fractured-controlled reservoirs of active and fossil geothermal systems (Patrier *et al.*, 1996; Papapanagiotou *et al.*, 1995; Ji and Browne, 2000; Mas *et al.*, 2003) are similar to the features observed in the Athabasca illites.

The relationship between increase in size of illite crystals and the *cv*-1*M*/*tv*-1*M* ratio has also been observed in sandstones from the North Sea (Lanson *et al.*, 1996, 2002). This creates questions regarding the mechanism of the *tv*-1*M* to *cv*-1*M* transition with coarsening of illite particles. However, the apparent difficulty in *tv*-1*M* polytype fibrous illites becoming coarser (*i.e.* in growing further) may be related to the concept that such a fibrous crystal habit of illite is only metastable.

CONCLUSIONS

From the data and information presented in this study on the clay mineral alteration around the Shea Creek U deposit, and after validation of our model with other deposits, illite could be used at different scales, from regional to local, as a pathfinder mineral in exploration for unconformity-type U deposits in the Athabasca Basin.

At a regional scale (tens of kilometers), the illitization process may be a distal signature of the fluid/rock interactions associated with U transport and deposition. The 'degree of illitization', in the absence of K-feldspars and the textural and structural characteristics of the illite may be indicators of distance from alteration zones at the sub-Athabasca unconformity. The term 'degree of illitization' represents the proportion of replacement of kaolin by illite and not the absolute quantity of illite. The regions in which kaolin is totally replaced by illite are typically located in the vicinity of the structures which focused the solutions responsible for the host-rock alteration.

At a local scale (hundreds of meters), the textural and structural characteristics of illite provide evidence of fluids, oversaturated with respect to illite, associated with U deposition. The *tv*-1*M* illite is a metastable phase indicator of the proximity to major flow channels. It can also be used to reconstruct the paleohydrodynamic constraints (fluid flow regime) at the regional scale.

Differences in crystallography and textural properties between 'diagenetic' regional illite and alteration illite restricted close to the unconformity or fractured zones, which focused the mineralizing fluids, have already been noticed in other unconformity-related U deposits. Beaufort *et al.* (2005) identified $2M_1$ diagenetic illite in the East Alligator Rivers Uranium Field, while illite restricted to altered levels was mainly of *tv*-1*M* polytype (± *cv*-1*M*). As in the present case, the control and mechanism of polytype transitions are still questionable.

ACKNOWLEDGMENTS

The research for this paper was supported financially by the exploration division of COGEMA. We thank all of the COGEMA geologists for sharing their knowledge of the geology of this part of the Athabasca Basin, and who participated in sample collection. We gratefully acknowledge Michel Cuney, Bruno Lanson, Derek Bain, Douglas K. McCarty and an anonymous reviewer for their critical reviews and very constructive comments.

REFERENCES

Bailey, S.W. (1980) Structure of layer silicates. Pp. 1–124 in: *Crystal Structure of Clay Minerals and their X-ray Identification* (G.W. Brindley and G. Brown, editors). Monograph **5**, Mineralogical Society, London.

Beaufort, D., Cassagnabère, A., Petit, S., Lanson, B., Berger, G., Lacharpagne, J.C. and Johansen, H. (1998) Kaolinite to dickite reaction in sandstone reservoirs. *Clay Minerals*, **33**, 297–316.

Beaufort, D., Patrier, P., Laverret, E., Bruneton, P. and Mondy, J. (2005) Clay alteration associated with Proterozoic unconformity-type uranium deposits in the East Alligator Rivers Uranium Field (Northern Territory, Australia). *Economic Geology*, **100**, 515–536.

Berger, G., Lacharpagne, J.C., Velde, B., Beaufort, D. and Lanson, B. (1997) Kinetic constraints on illitization reactions and the effects of organic diagenesis in sandstone/shale sequences. *Applied Geochemistry*, **12**, 23–35.

Bjorlykke, K. and Aagaard, P. (1992) Clay minerals in North Sea sandstones. Pp. 65–80 in: *Origin, Diagenesis and Petrophysics of Clay Minerals in Sandstones* (D.W. Houseknecht and E.D. Pittman, editors). Special Publication, Society for Sedimentary Geology.

Brindley, G.W. (1980) Order-disorder in clay mineral structures. Pp. 125–196 in: *Crystal Structures of Clay Minerals and their X-ray Identification* (G.W. Brindley and G. Brown, editors). Monograph **5**, Mineralogical Society, London.

Brouand, M. and Cuney, M. (2002) Age and nature of the plutonism of the western part of the Athabasca basin basement (northern Saskatchewan, Canada). *GAC-MAC joint annual meeting*, Saskatoon, Canada, Abstract Volume **27**, p. 14.

Brouand, M., Cuney, M. and Deloule, E. (2003) Eastern extension of the Taltson orgenic belt and eastern provenance of Athabasca sandstone: IMS 1270 ion microprobe U/Pb dating of zircon from concealed basement plutonic rocks and from overlying sandstone (Canada). Pp. 91–94 in: *Uranium Geochemistry* (M. Cuney, editor). International Conference Proceedings, Nancy.

Card, C.D. (2002) Basement rocks to the Western Athabasca basin. *GAC-MAC Joint Annual Meeting*, Saskatoon, Abstracts volume **27**, p. 17.

Champion, D. (1989) Etude des mécanismes de transformation des interstratifiés illite-smectite au cours de la diagenèse. PhD thesis, Université d'Orsay – Paris XI, France, 204 pp.

Chiarenzelli, J., Aspler, L., Villeneuve, M. and Lewry, J. (1998) Early Proterozoic evolution of the Saskatchewan

Craton and its allochthonous cover, Trans-Hudson Orogen. *The Journal of Geology*, **106**, 247–267.

Clauer, N. and Chaudhuri, S. (1995) *Clays in Crustal Environments. Isotope Tracing and Dating*. Springer-Verlag, Berlin, 358 pp.

Cumming, G.L., Krstic, D. and Wilson, J.A. (1987) Age of the Athabasca Group, Northern Alberta. *GAC-MAC Joint Annual Meeting*, Saskatoon 1987, Abstracts volume **12**, p. 35.

Cuney, M., Brouand, M., Cathelineau, M., Derome, D., Freiberger, R., Hecht, L., Kister, P., Lobaev, V., Lorilleux, G., Peiffert, C. and Bastoul, A.M. (2003) What parameters control the high grade-large tonnage of the Proterozoic unconformity related uranium deposits? Pp. 123–126 in: *Uranium Geochemistry* (M. Cuney, editor). International Conference Proceedings, Nancy.

Derome, D., Cathelineau, M., Cuney, M. and Fabre, C. (2003) Reconstruction of P, T, X characteristics of paleofluids in the McArthur River unconformity-type uranium deposit (Saskatchewan, Canada). Pp. 141–144 in: *Uranium Geochemistry* (M. Cuney, editor). International Conference Proceedings, Nancy, France.

Drits, V.A. and McCarty, D.K. (1996) The nature of diffraction effects from illite and illite-smectite consisting of interstratified trans-vacant and cis-vacant 2:1 layers: A semi-quantitative technique for determination of layer-type. *American Mineralogist*, **81**, 852–863.

Drits, V.A., Weber, F., Salyn, A.L. and Tsipursky, S.I. (1993) X-ray identification of one-layer illite varieties: application to the study of illites around uranium deposits of Canada. *Clays and Clay Minerals*, **41**, 389–398.

Ehrenberg, S.N., Aagaard, P., Wilson, M.J., Fraser, A.R. and Duthie, D.M.L. (1993) Depth-dependent transformation of kaolinite to dickite in sandstones of Norwegian continental shelf. *Clay Minerals*, **28**, 325–352.

Ey, F., Gauthier-Lafaye, F., Lillié, F. and Weber, F. (1985) A uranium unconformity deposit: The geological setting of the D orebody (Saskatchewan-Canada). Pp. 121–128 in: *The Carswell Structure Uranium Deposits, Saskatchewan* (R. Lainé, D. Alonso, and M. Svab, editors). Geological Association of Canada Special Paper, **29**.

Frey, M. and Robinson, D. (1999) *Low-Temperature Metamorphism*. Blackwell Science, Oxford, UK, 313 pp.

Gustafson, L.B. and Curtis, L.W. (1983) Post-Kombolgie metasomatism at Jabiluka, Northern Territory, Australia, and its significance in the formation of high grade uranium mineralization in lower Proterozoic rocks. *Economic Geology*, **35**, 26–56.

Güven, N. (2001) Mica structure and fibrous growth of illite. *Clays and Clay Minerals*, **49**, 189–196.

Güven, N., Hower, W.F. and Davies, D.K. (1980) Nature of authigenic illites in sandstone reservoirs. *Journal of Sedimentary Petrology*, **50**, 761–766.

Halter, G. (1988) Zonalité des altérations dans l'environnement des gisements d'uranium associés à la discordance du Proterozoïque moyen (Saskatchewan, Canada). PhD thesis, Université de Strasbourg, France, 253 pp.

Hoeve, J. and Quirt, D. (1984) *Uranium mineralization and host rock alteration in relation to clay mineral diagenesis and evolution of the middle-Proterozoic Athabasca Basin, Northern Saskatchewan, Canada*. Saskatchewan Research Council, Canada, Report **187**, 187 pp.

Hoeve, J. and Quirt, D. (1987) A stationary redox front as a critical factor in the formation of high grade unconformity-type uranium ores in the Athabasca basin, Saskatchewan, Canada. *Bulletin de Minéralogie*, **110**, 157–171.

Hoeve, J. and Sibbald, T.I.I. (1978) On the genesis of Rabbit Lake and other unconformity-type uranium deposits in northern Saskatchewan, Canada. *Economic Geology*, **73**, 1450–1473.

Hoeve, J., Quirt, D. and Alonso, D. (1985) Clay mineral stratigraphy of the Athabasca Group: Correlation inside and outside the Carswell Structure. Pp. 19–31 in: *The Carswell Structure Uranium Deposits, Saskatchewan* (R. Lainé, D. Alonso and M. Svab, editors). Geological Association of Canada Special Paper **29**.

Ji, J.F. and Browne, P.R.L. (2000) Relationship between illite crystallinity and temperature in active geothermal systems of New Zealand. *Clay and Clay Minerals*, **48**, 139–144.

Kister, P., Laverret, E., Quirt, D., Cuney, M., Patrier Mas, P., Beaufort, D. and Bruneton, D. (2006) Mineralogy and geochemistry of the host-rock alterations associated with the Shea Creek unconformity-type uranium deposits (Saskatchewan, Canada). Part 2. Regional scale spatial distribution of the Athabasca Group sandstone matrix minerals. *Clays and Clay Minerals*, **54**, 295–313.

Komninou, A. and Sverjensky, D.A. (1996) Geochemical modeling of the formation of an unconformity-type uranium deposit. *Economic Geology*, **91**, 590–606.

Kotzer, T.G. and Kyser, T.K. (1995) Petrogenesis of the Proterozoic Athabasca basin, Northern Saskatchewan, Canada, and its relation to diagenesis, hydrothermal uranium mineralization and paleohydrogeology. *Chemical Geology*, **120**, 45–89.

Kübler, B. (1964) Les argiles, indicateur de métamorphisme. *Revue de l'Institut Français du Pétrole*, **19**, 1093–1112.

Lanson, B. (1997) Decomposition of X-ray diffraction patterns (profile fitting): A convenient way to study clay minerals. *Clays and Clay Minerals*, **45**, 132–146.

Lanson, B., Beaufort, D., Berger, G., Baradat, J. and Lacharpagne, J.C. (1996) Illitization of diagenetic kaolinite-to-dickite conversion series: late stage diagenesis of the Lower Permian Rotliegend sandstone reservoir, off-shore of The Netherlands. *Journal of Sedimentary Research*, **66**, 501–518.

Lanson, B., Beaufort, D., Berger, G., Bauer, A., Cassagnabère, A. and Meunier, A. (2002) Authigenic kaolin and illitic minerals during burial diagenesis of sandstones: a review. *Clay Minerals*, **37**, 1–22.

Laverret, E. (2002) Evolutions spatiales et temporelles des altérations argileuses des gisements d'uranium associés à des discordances Protérozoïques. Partie Ouest du bassin de l'Athabasca, Canada. PhD thesis, Université de Poitiers, France, 192 pp.

Laverret, E., Patrier, P., Beaufort, D., Clauer, N., Bruneton, P. and Mondy, J. (2003) Time-space evolution of alterations in the unconformity-type uranium deposit of the Shea Creek prospect (Athabasca Basin, Canada). Pp. 211–214 in: *Uranium Geochemistry* (M. Cuney, editor). International Conference Proceedings, Nancy.

Liewig, N., Clauer, N. and Sommer, F. (1987) Rb-Sr and K-Ar dating of clay diagenesis in Jurassic sandstone oil reservoirs, North Sea. *American Association of Petroleum Geologists Bulletin*, **71**, 1467–1474.

Lorilleux, G., Jebrak, M., Cuney, M. and Baudemont, D. (2002) Polyphase hydrothermal breccias associated with unconformity-type uranium mineralization (Canada): from fractal analysis to structural significance. *Journal of Structural Geology*, **24**, 323–338.

Mas, A., Patrier, P., Beaufort, D. and Genter, A. (2003) Clay-mineral signatures of fossil and active hydrothermal circulations in the geothermal system of Lamentin Plain, Martinique. *Journal of Volcanology and Geothermal Research*, **124**, 195–218.

Moore, D.M. and Reynolds, R.C. (1989) Identification of mixed layered minerals. Pp. 241–269 in: *X-ray Diffraction and the Identification and Analyses of Clay Minerals* (D.M. Moore and R.C. Reynolds, editors). Oxford University Press, UK.

Pagel, M. (1975) Détermination des conditions physico-chimiques de la silicification diagénétique des grès Athabasca (Canada) au moyen des inclusions fluides. *Compte rendus de l'Académie des Sciences*, **280**D, 2301–2304.

Pagel, M. and Svab, M. (1985) Petrographic and geochemical variations within the Carswell structure metamorphic core and their implications with respect to uranium mineralization. Pp. 55–70 in: *The Carswell Structure Uranium Deposits, Saskatchewan* (R. Lainé, D. Alonso and M. Svab, editors). Special Paper **29,** Geological Association of Canada.

Papanagiotou, P., Patrier, P., Beaufort, D., Fouillac, A.M. and Rojas, J. (1995) Occurrence of smectite and smectite-rich mixed-layers at high temperature within reservoirs of active geothermal fields. *Proceedings of the World Geothermal Congress*, Florence, Italy, pp. 1071–1076.

Patrier, P., Papapanagiotou, P., Beaufort, D., Traineau, H., Bril, H. and Rojas, J. (1996) Role of permeability versus temperature in the distribution of the fine (<0.2 μm) clay fraction in the Chipilapa geothermal system (El Savador, Central America). *Journal of Volcanology and Geothermal Research*, **72**, 101–120.

Patrier, P., Beaufort, D., Laverret, E. and Bruneton, P. (2003) Dickite and $2M_1$ illite in deeply buried sandstones from the middle Proterozoic Kombolgie Formation (Northern Territory, Australia). *Clays and Clay Minerals*, **51**, 102–116.

Quirt, D.H. (1997) Geochemistry, host-rock alteration, mineralization, and uranium metallogenesis of the Wollaston EAGLE project area. In: *Thermotectonic and Uranium Metallogenetic Evolution of the Wollaston EAGLE Project Area* (I.R. Annesley, C. Madore, R. Shi and D.H. Quirt, editors). Saskatchewan Research Council, Publication No. R-1240-2-C-97, Part 2, 98 pp.

Quirt, D.H. (2003) Athabasca unconformity-type uraniuim deposits: one deposit type with many variations. Pp. 309–312 in: *Uranium Geochemistry* (M. Cuney, editor). International Conference Proceedings, Nancy, France.

Raffensperger, J.P. and Garven, G. (1995) The formation of unconformity-type uranium ore deposits 2. Coupled hydrochemical modelling. *American Journal of Science*, **295**, 639–696.

Rainbird, R.H., Stern, R.A. and Jefferson, C.W. (2002) Summary of detrital zircon geochronology of the Athabasca Group, Northern Saskatchewan and Alberta. In: *Summary of Investigations*, Saskatchewan Geological Survey, Saskatchewan Energy Mines, **2**, D-17, 3 pp.

Ramaekers, P. (1990) *Geology of the Athabasca Group (Helikian) in Northern Saskatchewan*. Saskatchewan Energy and Mines, Saskatchewan Geological Survey, Technical report **195**, 49 pp.

Ramaekers, P., Yeo, G. and Jefferson, C. (2001) Preliminary overview of regional stratigraphy in the Late Paleoproterozoic Athabasca Basin, Saskatchewan and Alberta. In: *Summary of Investigations.* Saskatchewan Geological Survey, Saskatchewan Energy Mines, **2**, pp. 240–251.

Renac, C., Kyser, T.K., Durocher, K., Dreaver, G. and O'Connor, T. (2002) Comparison of diagenetic fluids in the Proterozoic Thelon and Athabasca basins, Canada: implications for a long protracted fluid history in stable intracratonic basins. *Canadian Journal of Earth Sciences*, **39**, 113–132.

Reynolds, R.C. (1985) *Description of program NEWMOD for the calculation of the one-dimensional X-ray diffraction patterns of mixed-layered clays*. Department of Earth Sciences, Dartmouth College, Hanover, New Hampshire, 23 pp.

Reynolds, R.C. (1993) Three-dimensional X-ray powder diffraction from disordered illite: simulation and interpretation of the diffraction patterns. Pp. 44–78 in: *Computer Applications to X-ray Powder Diffraction Analysis of Clay Minerals* (R.C. Reynolds and J.R. Walker, editors). Workshop Lectures, vol. **5**, The Clay Minerals Society, Boulder, Colorado.

Rippert, J.C., Koning, E., Robbins, J., Koch, R. and Baudemont, D. (2000) The Shea Creek uranium project, West Athabasca basin, Saskatchewan, Canada. In: *Proceedings, GeoCanada2000, the Millenium Geoscience Summit, Calgary.* GAC-MAC joint annual meeting, abstract 570.

Środoń, J. and Eberl, D.D. (1984) Illite. Pp. 495–544 in: *Micas* (S.W. Bailey, editor). Reviews in Mineralogy, **13**. Mineralogical Society of America, Washington, D.C.

(*Received 31 May 2004; revised 23 December 2005; Ms. 920; A.E. Bruno Lanson*)